Paleoceanography and Paleoclimatology

RESEARCH ARTICLE
10.1029/2019PA003646

An ~130 kyr Record of Surface Water Temperature and $\delta^{18}O$ From the Northern Bay of Bengal: Investigating the Linkage Between Heinrich Events and Weak Monsoon Intervals in Asia

Stefan Lauterbach[1,2], Nils Andersen[1], Yiming V. Wang[2,3], Thomas Blanz[2], Thomas Larsen[1,3], and Ralph R. Schneider[1,2]

[1]Leibniz Laboratory for Radiometric Dating and Stable Isotope Research, Kiel University, Kiel, Germany, [2]Institute of Geosciences, Kiel University, Kiel, Germany, [3]Department of Archaeology, Max Planck Institute for Science of Human History, Jena, Germany

Key Points:
- A paired record of planktonic foraminifera $\delta^{18}O$ and $U^{K'}_{37}$-based sea surface temperature (SST) from the northern Bay of Bengal is provided
- Short-term reductions in Indian Summer Monsoon (ISM) precipitation occurred parallel to North Atlantic Heinrich events
- Reductions in ISM precipitation during the last ~130 kyr were apparently not always connected to changes in Bay of Bengal SST

Correspondence to:
S. Lauterbach,
slauterbach@leibniz.uni-kiel.de

Citation:
Lauterbach, S., Andersen, N., Wang, Y. V., Blanz, T., Larsen, T., & Schneider, R. R. (2020). An ~130 kyr record of surface water temperature and $\delta^{18}O$ from the northern Bay of Bengal: Investigating the linkage between Heinrich events and Weak Monsoon Intervals in Asia. *Paleoceanography and Paleoclimatology*, *35*, e2019PA003646. https://doi.org/10.1029/2019PA003646

Received 2 MAY 2019
Accepted 29 JAN 2020
Accepted article online 31 JAN 2020

Abstract Millennial-scale reductions in monsoon precipitation, so-called Weak Monsoon Intervals (WMIs), have been identified in numerous paleoclimate records across the Afro-Asian monsoon domain throughout the last glacial-interglacial cycle. These are considered the regional response to cooling during Heinrich events in the North Atlantic realm and several mechanisms have been suggested to explain this hemisphere-scale climatic teleconnection. In particular, reductions in Indian Ocean sea surface temperature (SST) have been proposed as the linking element between Heinrich events and WMIs. However, the validity of this relationship has only been demonstrated for the last ~20 kyr, leaving unresolved whether it also holds on longer time scales. Here we present a new paired record of planktonic foraminifera-based $\delta^{18}O_{sw\text{-}ivc}$ and $U^{K'}_{37}$-based SST from the northern Bay of Bengal, covering the last ~130 kyr. The $\delta^{18}O_{sw\text{-}ivc}$ record clearly reflects orbitally paced changes of Indian Summer Monsoon intensity superimposed by centennial- to millennial-scale WMIs that occurred synchronously to North Atlantic Heinrich events. Comparison with the $U^{K'}_{37}$-based SST reconstruction reveals, however, that WMIs in most cases were not paralleled by ocean surface cooling, questioning whether Indian Ocean SST lowering was the linking element between Heinrich events and reductions in monsoon precipitation in Asia also during the last glacial period.

1. Introduction

Understanding teleconnections and feedback mechanisms in the global climate system in the past is of key importance for better forecasting its behavior under future global warming scenarios and how this may affect modern societies and economies. This is particularly true for the Asian monsoon system, whose variability influences the daily life of billions of people and thus also global economy (e.g., Gadgil & Rupa Kumar, 2006). Existing knowledge about the long-term evolution of the Indian Summer Monsoon (ISM) and the East Asian Summer Monsoon (EASM) under different to modern climatic boundary conditions is mainly based on the investigation of speleothems from India (Kathayat et al., 2016) and China (e.g., Cai et al., 2015; Cheng et al., 2016; Wang et al., 2001) as well as marine sediments from the Arabian Sea (e.g., Clemens & Prell, 2003; Deplazes et al., 2014; Rostek et al., 1993; Schulz et al., 1998), South China Sea (e.g., Huang et al., 2018; Thomas et al., 2014; Wang et al., 1999), and the tropical Indian Ocean (e.g., Bolton et al., 2013; Mohtadi et al., 2010). On long time scales, particularly the Chinese speleothem records indicate a direct influence of Northern Hemisphere summer insolation, that is, changes in the Earth's orbital parameters, on Asian monsoon variability (e.g., Cheng et al., 2016), but this view is still under debate (Caley et al., 2011; Caley et al., 2014; Clemens et al., 2010). On shorter, that is, (multi)millennial, time scales there is in contrast evidence for a strong synchroneity between abrupt climate events in the North Atlantic realm and the Asian monsoon system (e.g., Deplazes et al., 2013; Wang et al., 2005), pointing toward a close hemisphere-scale teleconnection between both regions. In this context, multiple paleoclimate archives across the Afro-Asian monsoon domain have provided evidence for centennial- to millennial-scale reductions in monsoon precipitation, so-called Weak Monsoon Intervals (WMIs), which occurred synchronously to cold intervals in the North Atlantic realm, for example, during Heinrich events (e.g., Cheng et al., 2016;

Colin et al., 1998; Deplazes et al., 2014; Kathayat et al., 2016; Mingram et al., 2018; Stager et al., 2011; Wang et al., 2001). However, the exact mechanisms behind this teleconnection and thus the drivers that could control possible future monsoon failures are still debated.

Climate simulations have proposed, for example, (1) a combination of a stationary Rossby wave train teleconnection and a circulation anomaly in the westerly jet over northern Africa and western India (Mohtadi et al., 2014) or (2) perturbations in the position of the Northern Hemisphere subtropical westerly jet, driven by sea surface temperature (SST) anomalies in the tropical Atlantic Ocean (Marzin et al., 2013), as the linking element between abrupt cold events in the North Atlantic realm and reduced monsoon precipitation in Asia. Alternatively, also reduced SSTs in the Indian Ocean in response to a general cooling of the Northern Hemisphere, driven by increasing sea ice extent in the North Atlantic, could represent the link between North Atlantic Heinrich events and WMIs (Pausata et al., 2011). Especially the latter mechanism is corroborated by proxy data from the Arabian Sea, confirming substantial ocean surface water cooling and associated monsoon weakening during the two most recent North Atlantic cold spells, the Younger Dryas and Heinrich event H1 (Tierney et al., 2016). However, other proxy records from the Arabian Sea as well as from the Bay of Bengal (BoB) indicate no particular cooling but a warming of the Indian Ocean surface waters at the time of the Younger Dryas and Heinrich events H1 and H2 (Anand et al., 2008; Panmei et al., 2017; Saher et al., 2007; Saraswat et al., 2013), thus questioning the general validity of the proposed linkage between ISM weakening and Indian Ocean surface water cooling. So far, most of the available paleoceanographic proxy records from the core zone of the ISM, that is, the BoB and the adjacent Andaman Sea (e.g., Ahmad et al., 2012; Contreras-Rosales et al., 2014; Gebregiorgis et al., 2016; Govil & Naidu, 2011; Kudrass et al., 2001; Marzin et al., 2013; Rashid et al., 2007; Rashid et al., 2011; Raza et al., 2017; Sijinkumar et al., 2016) cover only the Holocene and latest Pleistocene (<50 kyr) and/or have a relatively low temporal resolution. This largely limits the proper reconstruction of short-term ISM variability in this region under climatic boundary conditions different than today, particularly during the last glacial and last interglacial periods. Hence, new proxy records that (1) cover a full glacial-interglacial cycle and (2) have a sufficient temporal resolution are needed to improve our understanding of past ISM dynamics and reliably assess the relationship between Indian Ocean SST and WMIs.

In this study we present new proxy records of monsoon-driven paleoceanographic changes during the last ~130 kyr from the northern BoB. In particular, we investigate the manifestation of WMIs in this part of the Indian Ocean during the entire last glacial-interglacial cycle as recorded by the stable oxygen isotope composition of planktonic foraminifera, reflecting changes in monsoonal precipitation-derived freshwater runoff. By comparing these data with a parallel alkenone-based SST reconstruction, we investigate whether WMIs occurred synchronously to sea surface water cooling in the northern BoB and discuss the linkage between WMIs and North Atlantic Heinrich events.

2. Study Area and Investigated Sediment Material

The BoB constitutes the northeastern part of the Indian Ocean between the Indian subcontinent, Myanmar, and the Andaman and Nicobar Islands, which is approximately between 6°N and 22°N and 80°E and 92–94°E. Gravity Core SO 188-17286-1 (henceforth denoted 17286-1) was retrieved from its northernmost part during R/V *Sonne* cruise SO 188 (*Bengal Sea Level*; Spieß et al., 2006). The coring site is located on the continental slope off Bangladesh (19°44.58′N, 89°52.76′E, 1428 m water depth; Figure 1), ~220 km south of the mouth of the Ganges-Brahmaputra-Meghna (GBM) river system and ~80 km east of the "Swatch of No Ground", a deeply incised canyon on the Bengal Shelf (Spieß et al., 2006). Two other sediment cores, which were investigated by Kudrass et al. (2001; SO 93-126KL) and Contreras-Rosales et al. (2014; SO 188-342KL), are located ~30 km to the northeast. Instead of being transported laterally across the slope, most of the sediment drift upon the Bengal Shelf is deflected towards and funneled into the "Swatch of No Ground" from where is transported by turbidity currents to the deeper Bengal Fan (Contreras-Rosales et al., 2014; Weber et al., 2003). As a consequence, sedimentation at the study site is predominantly hemipelagic. Gravity Core 17286-1 is 984 cm long and consists of hemipelagic yellowish brown silty clay with a few mollusk shells (>1 mm) in the uppermost part while olive gray nannofossil-rich clay with abundant foraminifera and mollusk shells dominates the lower part (Spieß et al., 2006).

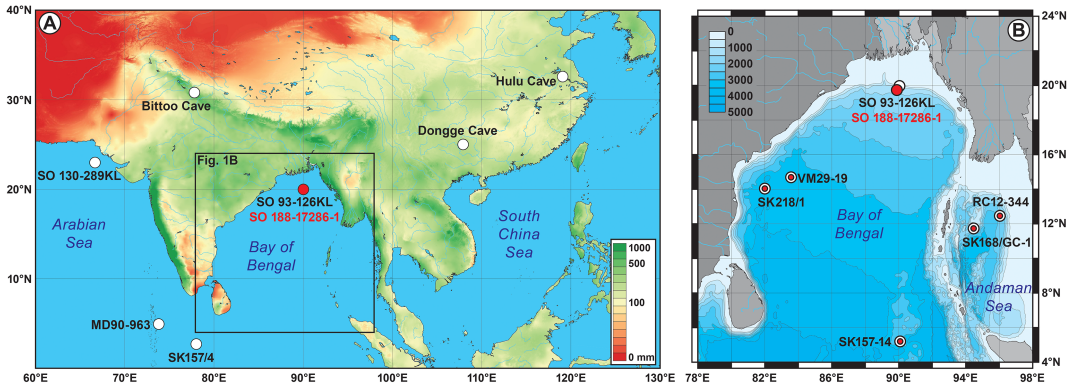

Figure 1. (a) Map of the Asian monsoon domain with average July precipitation (WorldClim1 30 in. gridded precipitation data; Hijmans et al., 2005) and the location of Core 17286-1 (red dot) and other proxy records of past monsoon variability (white dots) that are partly displayed in Figure 5 and discussed in the text. (b) Detailed bathymetric map of the BoB (water depth in meters below sea level) with the location of Core 17286-1 (red dot) and other regional sea surface temperature (SST) records (red-white dots) that are displayed in Figure 6 and discussed in the text.

The present-day oceanographic and depositional regime in the northern BoB is mainly controlled by the inflow of the GBM river system, which has a catchment of ~1.7×10^6 km^2 and drains large parts of ISM core zone, that is, the Himalayas and the northern Indian subcontinent. Besides providing large amounts of allochthonous sediment to the Bengal Shelf, the GBM river system also discharges enormous volumes of freshwater from monsoon precipitation into the northern BoB (on average ~1120 km^3 yr^{-1}; Milliman & Farnsworth, 2011). This is, in addition to the general excess of precipitation over evaporation across the BoB, responsible for a relatively low sea surface salinity in the area (Sen Gupta & Naqvi, 1984). Furthermore, due to the massive riverine input of rainfall-derived freshwater during the monsoon and post-monsoon season in summer and autumn, when discharge can reach peak values in the range of 10^5 m^3 s^{-1} (Milliman & Farnsworth, 2011), sea surface salinity around the coring site (grid 19–20°N, 89–90°E) shows a distinct seasonality with significantly lower values during summer (~27–31 PSU) than during winter (~31–32 PSU) (Boyer et al., 2013). Freshwater input also affects the stable oxygen isotope composition of the ocean surface water ($\delta^{18}O_{sw}$) in the northern BoB. In particular, more negative $\delta^{18}O_{sw}$ values can be expected during predominantly wet climate conditions (e.g., during and/or shortly after the monsoon season) when the discharge of ^{18}O-depleted freshwater by the GBM river system is higher, which is largely confirmed by observational data (Delaygue et al., 2001; Sengupta et al., 2013; Singh et al., 2010). Recent (1955–2012) SST at the coring site varies between ~25.5–26.5 °C in winter (January to March) and ~28.8–29.2 °C in summer (July to September) with an annual mean of ~27.8–28.2 °C (Boyer et al., 2013).

3. Methods

3.1. δ^{18}O Analyses of Benthic and Planktonic Foraminifera

To establish a chronology for Core 17286-1 (see section 3.2) and to investigate paleoceanographic and paleoclimatic changes at the coring site, the stable oxygen isotope composition of benthic ($\delta^{18}O_{benthic}$) and planktonic foraminifera ($\delta^{18}O_{planktonic}$) was determined at the Leibniz Laboratory for Radiometric Dating and Stable Isotope Research at Kiel University. For these analyses, 1 cm thick slices of bulk sediment (sample increment 4–6 cm) were taken from Core 17286-1 and subsequently washed and sieved to retrieve the foraminifera. Tests of planktonic (*Globigerinoides ruber* (white); size fraction 250–315 μm) and benthic foraminifera (*Uvigerina* spp.; size fraction 250–400 μm) from each of these subsamples were identified and handpicked under a microscope. For determining the δ^{18}O of the planktonic foraminifera, at least 30 tests per sediment subsample were selected and subsequently analyzed with a Finnigan MAT 251 isotope ratio mass spectrometer (IRMS) coupled to a Kiel I (prototype) carbonate preparation device. The δ^{18}O of the benthic foraminifera (1–12 specimens per sample; samples with more than six specimens were homogenized and split prior to analysis) was determined with a Thermo Fisher Scientific MAT 253 IRMS coupled to a Kiel IV carbonate preparation device. For all measurements, the calcitic foraminifera tests were reacted with 100% H_3PO_4 at 75 °C under vacuum and the evolved CO_2 was analyzed eight times with the IRMS. The

Table 1
AMS ^{14}C Dates Obtained From Mixed Planktonic Foraminifera Samples From Core 17286-1

Sample/lab code	Core depth (cm)	AMS ^{14}C age (a BP ± σ)	Calibrated age (cal. a BP, 2σ)
KIA49929	2.5	1430 ± 40	923–1215
KIA49930	38.5	7135 ± 45	7554–7830
KIA49931	62.5	10,585 ± 60	11,688–12,432
KIA50521[a]	70.5	11,140 ± 60	12,577–12,873
KIA50520	81.5	11,320 ± 55	12,687–13,067
KIA50404	98.5	13,515 ± 65	15,552–16,128
KIA49933	118.5	14,665 ± 85	17,141–17,767
KIA50405	218.5	21,740 ± 180	25,334–26,044
KIA49934	248.5	24,320 ± 230	27,674–28,564
KIA49935	352.5	34,400 ± 800	36,464–40,430
KIA49936	368.5	35,650 ± 950	38,148–41,980
KIA50407	392.5	38,300 ± 1300	40,147–44,895
KIA49937	*428.5*	*>42670*	*n.d.*

Note. Conventional AMS ^{14}C ages were calibrated using OxCal 4.3 (Bronk Ramsey, 2009a) with the Marine13 calibration data set (Reimer et al., 2013) and a marine reservoir correction of 322 ^{14}C yr (R = 400 yr, ΔR = −78 ± 53 yr) for the northern BoB (Southon et al., 2002). Italicized samples have been omitted from Bayesian age modeling with OxCal 4.3.
[a]Small sample (<0.5 mg C).

resulting $\delta^{18}O$ values are reported relative to the Vienna Pee Dee Belemnite (VPDB) scale as defined through the NBS 19 standard. The analytical precision of repeated measurements of different internal and international standards (NBS 19, IAEA-603) was better than ±0.09‰ (1σ) and duplicate measurements of 21 samples of benthic foraminifera yielded an analytical precision better than ±0.07‰ (1σ).

3.2. Age Model Development

In order to establish an age model for Core 17286-1, the radiocarbon (^{14}C) ages of 13 samples of mixed planktonic foraminifera (*G. ruber*, *Globigerinoides trilobus*, *Globigerinoides sacculifer*; Table 1) were determined by accelerator mass spectrometry (AMS) ^{14}C dating at the Leibniz Laboratory for Radiometric Dating and Stable Isotope Research at Kiel University. The obtained conventional AMS ^{14}C ages were calibrated using OxCal 4.3 (Bronk Ramsey, 2009a) with the Marine13 calibration curve (Reimer et al., 2013) and a marine reservoir correction of 322 ^{14}C yr (R = 400 yr, ΔR = −78 ± 53 yr) for the northern BoB (Southon et al., 2002). To further constrain the core chronology, particularly in the part beyond the range of ^{14}C dating (below ~400 cm core depth), we used the approach conventionally applied to Quaternary deep-sea sediments, that is, the correlation with a chronologically well-constrained $\delta^{18}O_{benthic}$ reference record. We therefore identified 11 characteristic stratigraphic tie points in the Core 17286-1 $\delta^{18}O_{benthic}$ record (see sections 3.1 and 4.1) and assigned to them the ages of corresponding points in the LS16 global $\delta^{18}O_{benthic}$ stack (Lisiecki & Stern, 2016; Table 2 and Figure 2). The final age model of Core 17286-1 was then established by Bayesian age modeling using a *P_Sequence* depositional model with variable parameter k and outlier analysis implemented in OxCal 4.3 (Bronk Ramsey, 2008, 2009a, 2009b; Bronk Ramsey & Lee, 2013). As model input parameters we used 12 of the 13 obtained AMS ^{14}C ages (the lowermost sample yielded an infinite ^{14}C age and was therefore discarded), the ages of the 11 stratigraphic tie points provided through correlation with the LS16 global $\delta^{18}O_{benthic}$ stack, and the date of the coring campaign (AD 2006) for the sediment surface (Figure 3). To consider the inherent chronological uncertainty of the LS16 global $\delta^{18}O_{benthic}$ stack, we also incorporated the published 2σ age uncertainties of the 11 tie points (Lisiecki & Stern, 2016) in the model.

3.3. Reconstruction of Past SST

To reconstruct past SST, we extracted long-chain alkenones from the Core 17286-1 sediments. These unsaturated methyl and ethyl ketones, which are mainly synthesized by the surface water-growing haptophyte algae *Emiliana huxleyi* and a few other related coccolithophore species (e.g., Marlowe et al., 1984; Volkman et al., 1980), are highly persistent and, due to the fact that *Emiliana huxleyi* is by far the most important primary producer of biogenic carbonate in the ocean, ubiquitous in Quaternary marine sediments (Marlowe et al., 1990). The ratio of the di-unsaturated and tri-unsaturated homologues of the alkenone n-C_{37} (n-$C_{37:2}$ and n-$C_{37:3}$), which is described as the alkenone n-C_{37} unsaturation index $U^{K'}_{37}$ (Prahl & Wakeham, 1987), is thereby largely dependent on the SST at the time of coccolithophore growth (e.g., Brassell et al., 1986; Marlowe et al., 1984; Müller et al., 1998; Prahl & Wakeham, 1987; Rosell-Melé et al., 1995; Sonzogni et al., 1997), enabling the reconstruction of past SST changes.

Lipid biomarkers were extracted from freeze-dried and homogenized sediment subsamples (~2 g sediment, 2 cm sampling interval) at the Institute of Geosciences at Kiel University by using a Dionex ASE 200 accelerated solvent extractor, operating in two cycles with a 9:1 (v/v) mixture of dichloromethane and methanol at 100 °C and 100 bar N_2 (g) pressure (cf. Rohde Krossa et al., 2017). Aliquots of the total lipid extract (1 or 2

Table 2
Tie Points in the Core 17286-1 $\delta^{18}O_{benthic}$ Record and Corresponding Ages in the LS16 Global $\delta^{18}O_{benthic}$ Stack (Lisiecki & Stern, 2016)

Tie point	17286-1 core depth (cm)	LS16 age (ka BP)
LS16 #1	102.5	18.0
LS16 #2	268.5	29.5
LS16 #3	362.5	38.0
LS16 #4	408.5	46.5
LS16 #5	498.5	54.5
LS16 #6	578.5	59.5
LS16 #7	698.5	75.0
LS16 #8	772.5	85.0
LS16 #9	868.5	103.5
LS16 #10	928.5	116.0
LS16 #11	968.5	132.0

Note. For a visualization of the correlation see Figure 2.

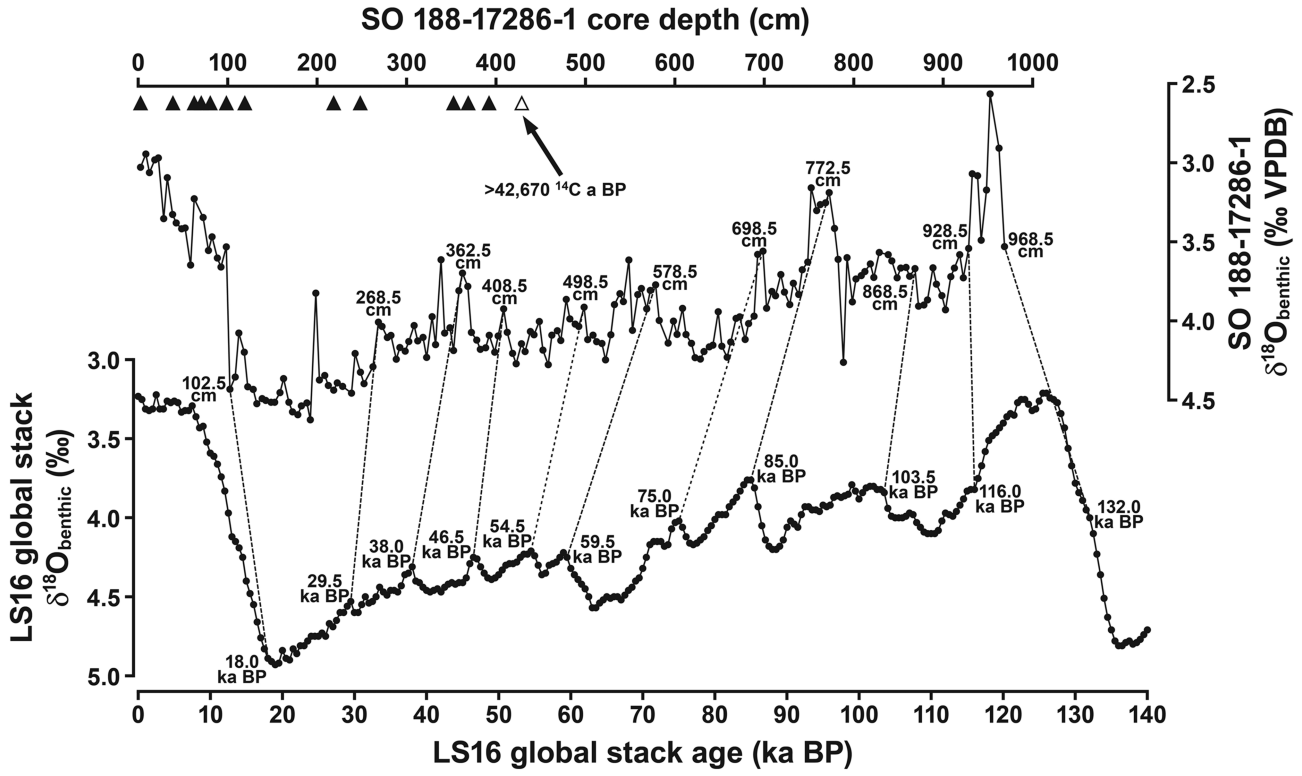

Figure 2. The Core 17286-1 $\delta^{18}O_{benthic}$ record (triangles beneath the depth scale indicate AMS ^{14}C dates) and its correlation with the LS16 global $\delta^{18}O_{benthic}$ stack (Lisiecki & Stern, 2016). Dashed lines indicate the position of the 11 tie points (with depths in Core 17286-1 and corresponding ages in the LS16 global $\delta^{18}O_{benthic}$ stack), which have been used to establish the age model for Core 17286-1 (see section 3.2 and Table 2).

μl, depending on the organic carbon content of the sediment subsamples) were subsequently analyzed for long-chain alkenones with a system of two sequentially coupled Agilent 6890 N gas chromatographs (double column multidimensional gas chromatography), allowing the separation and quantification of *n*-$C_{37:2}$ and *n*-$C_{37:3}$ (Etourneau et al., 2010). Quantification of the two compounds was achieved through addition of an internal standard (cholestane ($C_{37}H_{48}$) and hexatriacontane ($C_{36}H_{74}$)) and the alkenone unsaturation index $U^{K'}_{37}$ for each sample was finally calculated from the ratio between the concentrations of *n*-$C_{37:2}$ and *n*-$C_{37:3}$ according to the equation of Prahl and Wakeham (1987). The resulting $U^{K'}_{37}$ values where then converted into SST values using the equation SST (°C) = ($U^{K'}_{37}$ − 0.316) /0.023, which has been derived by Sonzogni et al. (1997) from a core top calibration study in the tropical and subtropical Indian Ocean (about 20°N to 45°S). This calibration equation was primarily developed for SSTs between 24 and 29 °C and considers seasonal variations in coccolithophore flux/productivity (Sonzogni et al., 1997). The analytical error of the measurements, based on replicate analyses of internal laboratory sediment standards, is <0.01 $U^{K'}_{37}$ units/<0.1 °C (1σ), and the error of the calibration data set is ±1.1 °C (Sonzogni et al., 1997).

3.4. Calculation of $\delta^{18}O_{sw\text{-}ivc}$ From $\delta^{18}O_{planktonic}$

In general, $\delta^{18}O_{planktonic}$ is influenced by superimposed changes in $\delta^{18}O$ of the ambient ocean surface water ($\delta^{18}O_{sw}$) and SST, with the former being mutually affected by changes in global ice volume and freshwater supply, either by river runoff or precipitation. To derive $\delta^{18}O_{sw}$ from measured $\delta^{18}O_{planktonic}$ and calculated SST, we used the relationship $\delta^{18}O_{sw}$ [‰] = ((SST − 14.9)/4.8) + $\delta^{18}O_{planktonic}$ (Bemis et al., 1998) and furthermore added 0.27‰ to convert the resulting $\delta^{18}O_{sw}$ values to the Vienna Standard Mean Ocean Water (VSMOW) scale. Finally, to obtain an ice volume-corrected record of the ocean surface water stable oxygen isotope composition ($\delta^{18}O_{sw\text{-}ivc}$), we subtracted the inherent effect of past global ice volume changes ($\Delta\delta^{18}O_{icevol}$; Figure 4) as published by Waelbroeck et al. (2002) (tuned to the chronology of the LS16 global $\delta^{18}O_{benthic}$ stack) from the calculated $\delta^{18}O_{sw}$ values.

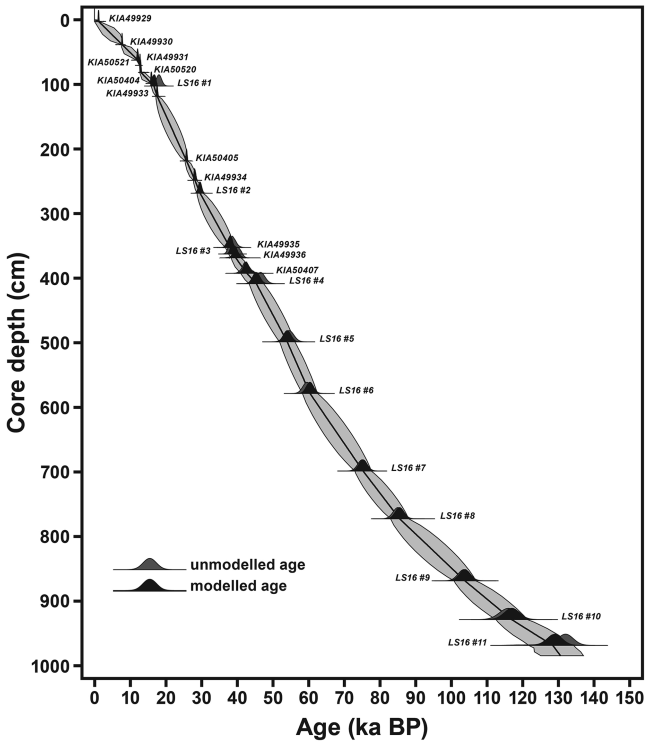

Figure 3. Age model of Core 17286-1 as derived from the *P_Sequence* depositional model implemented in OxCal 4.3 (Bronk Ramsey, 2008, 2009a, 2009b; Bronk Ramsey & Lee, 2013). The calibrated ages of the individual AMS ^{14}C dating samples (Table 1) and the ages of isotopic tie points derived from correlation of the $\delta^{18}O_{benthic}$ record with the LS16 global $\delta^{18}O_{benthic}$ stack (Lisiecki & Stern, 2016; Table 2) are displayed as 2σ probability functions. The solid black line and the gray shading represent the age model and its 2σ probability range, respectively.

4. Results

4.1. The $\delta^{18}O_{benthic}$ Record and Correlation With the LS16 global $\delta^{18}O_{benthic}$ Stack

Overall, the $\delta^{18}O_{benthic}$ record of Core 17286-1 reveals a pattern that is largely similar to the LS16 global $\delta^{18}O_{benthic}$ stack during the last ~130 kyr (Figure 2). This enables a proper correlation between both records (see section 3.2) and hence a fairly robust chronological control for the lower part of Core 17286-1 beyond the range of ^{14}C dating. Slight temporal offsets of <2 kyr between the Core 17286-1 $\delta^{18}O_{benthic}$ record and the LS16 global $\delta^{18}O_{benthic}$ stack during a few intervals are related to the Bayesian age modeling approach. Nevertheless, this is still within the 2σ uncertainty ranges of the Core 17286-1 age model (Figure 3) and the chronology of the LS16 global $\delta^{18}O_{benthic}$ stack. As deduced from the final age model of Core 17286-1, the average sedimentation rate is ~5 cm kyr^{-1} during Marine Isotope Stage (MIS) 1, ~11.5 cm kyr^{-1} during MIS 2, ~9.5 cm kyr^{-1} throughout MIS 3 and 4, ~5–6 cm kyr^{-1} throughout MIS 5a to 5d, and ~4 cm kyr^{-1} during MIS 5e. This yields a data resolution of ~300–1100 and ~100–550 yr for the $\delta^{18}O$ and SST record, respectively.

Throughout the record, $\delta^{18}O_{benthic}$ varies between ~2.6‰ and ~4.6‰ (Figures 4 and 5). Lowest values (~2.6–3.5‰) are observed between ~129 and ~117 ka BP, that is, during MIS 5e, followed by an interval of slightly higher values (~3.5–3.9‰) between ~117 and ~88 ka BP. A short-term episode of lower values (~3.2–3.4‰) is observed between ~88 and ~82 ka BP before $\delta^{18}O_{benthic}$ increases again to ~3.5–4.5‰ at the end of MIS 5b, fluctuating around 4.0‰ throughout MIS 4 to MIS 2. Highest $\delta^{18}O_{benthic}$ values (around 4.5‰) are reached at the end of MIS 2 (last glacial maximum (LGM)) before a sharp drop to lower values (<3.5‰) is observed at ~16 ka BP, marking the onset of the Postglacial (Figures 4 and 5).

4.2. Alkenone Concentration and Reconstructed SST

The sum concentration of *n*-$C_{37:2}$ and *n*-$C_{37:3}$ varies throughout the record between ~50 and >700 ng g^{-1} with the concentration of *n*-$C_{37:3}$ being in general one magnitude lower than that of *n*-$C_{37:2}$ (Figure 4). Characteristic are frequent multimillennial-scale fluctuations between intervals of high and low alkenone concentrations. The $U^{K'}_{37}$ index ranges between 0.802 and 0.989, yielding SST estimates between ~22.0 and ~29.2 °C (Figure 4). The SST reconstruction for the last ~130 kyr is characterized by a considerable short-term variability with occasional fluctuations of >1.5 °C within a few centuries. Changes in the sum concentration of *n*-$C_{37:2}$ and *n*-$C_{37:3}$ are apparently not correlated with changes in SST as low alkenone concentrations occur during intervals of both high and low SSTs (Figure 4). However, higher total alkenone concentrations (>200 ng g^{-1}) are observed only during intervals with SSTs exceeding 25.0 °C. In general, highest SSTs (>27.5 °C) are observed during intervals of interglacial and interstadial climate conditions, that is, during MIS 1 (since ~15 ka BP) and during MIS 5e to early MIS 5b (~129–89 ka BP), while slightly lower SSTs characterize the late MIS 5 as well as MIS 4 to MIS 2. SSTs significantly below 27.0 °C are only observed during late MIS 4 as well as throughout MIS 3 and MIS 2 with lowest values (<25.0 °C) occurring at ~51–46 and ~35–30 ka BP. The average Holocene (0–10 ka BP) SST is ~27.9 °C, while it reaches ~26.2 °C during the LGM (20–26 ka BP) and ~28.9 °C during MIS 5e (115–129 ka BP) (Figures 4 and 5).

4.3. The $\delta^{18}O_{planktonic}$ Record and Calculated $\delta^{18}O_{sw\text{-}ivc}$

The long-term pattern of the $\delta^{18}O_{planktonic}$ record is fairly similar to that of $\delta^{18}O_{benthic}$. Lowest $\delta^{18}O_{planktonic}$ values (below −3.5‰) are observed during MIS 5e prior to a distinct increase by ~1.5‰ starting at ~120 ka BP. Between ~117 and ~68 ka BP, $\delta^{18}O_{planktonic}$ ranges between about −3.0‰ and −1.5‰ with relatively low

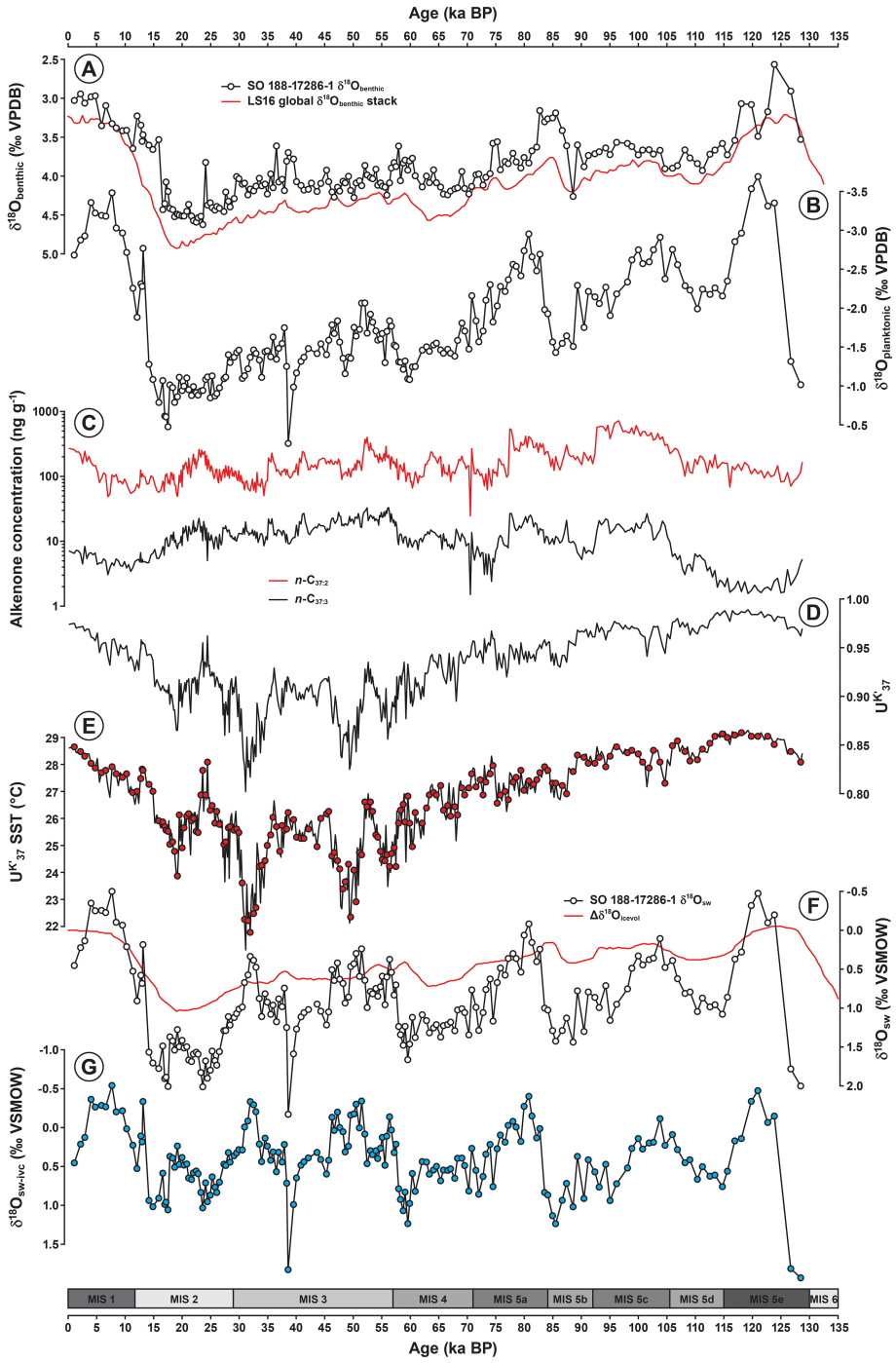

Figure 4. Proxy data obtained from Core 17286-1. (a) $\delta^{18}O_{benthic}$ obtained from *Uvigerina* spp. The LS16 global $\delta^{18}O_{benthic}$ stack (Lisiecki & Stern, 2016) is given for comparison. Note the partial temporal difference between the two records, which is owed to the age modeling procedure of Core 17286-1 (see sections 3.2 and 4.1). (b) $\delta^{18}O_{planktonic}$ obtained from *G. ruber* (white). (c) Concentrations of *n*-$C_{37:2}$ and *n*-$C_{37:3}$. Note the logarithmic scale. (d) U^{K}_{37} index. (e) SST calculated from the $U^{K'}_{37}$ index using the core top calibration established for the tropical and subtropical Indian Ocean by Sonzogni et al. (1997). Filled circles mark samples with parallel $\delta^{18}O_{planktonic}$ measurements that were used to calculate $\delta^{18}O_{sw\text{-}ivc}$. (f) $\delta^{18}O_{sw}$ (calculated from $U^{K'}_{37}$-based SST and $\delta^{18}O_{planktonic}$; for details see section 3.4) and $\Delta\delta^{18}O_{icevol}$ (Waelbroeck et al., 2002; tuned to the LS16 global $\delta^{18}O_{benthic}$ stack), which has been used to calculate $\delta^{18}O_{sw\text{-}ivc}$. (g) $\delta^{18}O_{sw\text{-}ivc}$ ($\delta^{18}O_{sw}$ corrected for the effect of global ice volume changes according to Waelbroeck et al. (2002); for details see section 3.4). Relatively higher $\delta^{18}O_{sw\text{-}ivc}$ values (note the reverse scale) reflect WMIs. Marine isotope stages (MIS) are given for comparison with boundaries following Lisiecki and Raymo (2005) and Martín-Puertas et al. (2014).

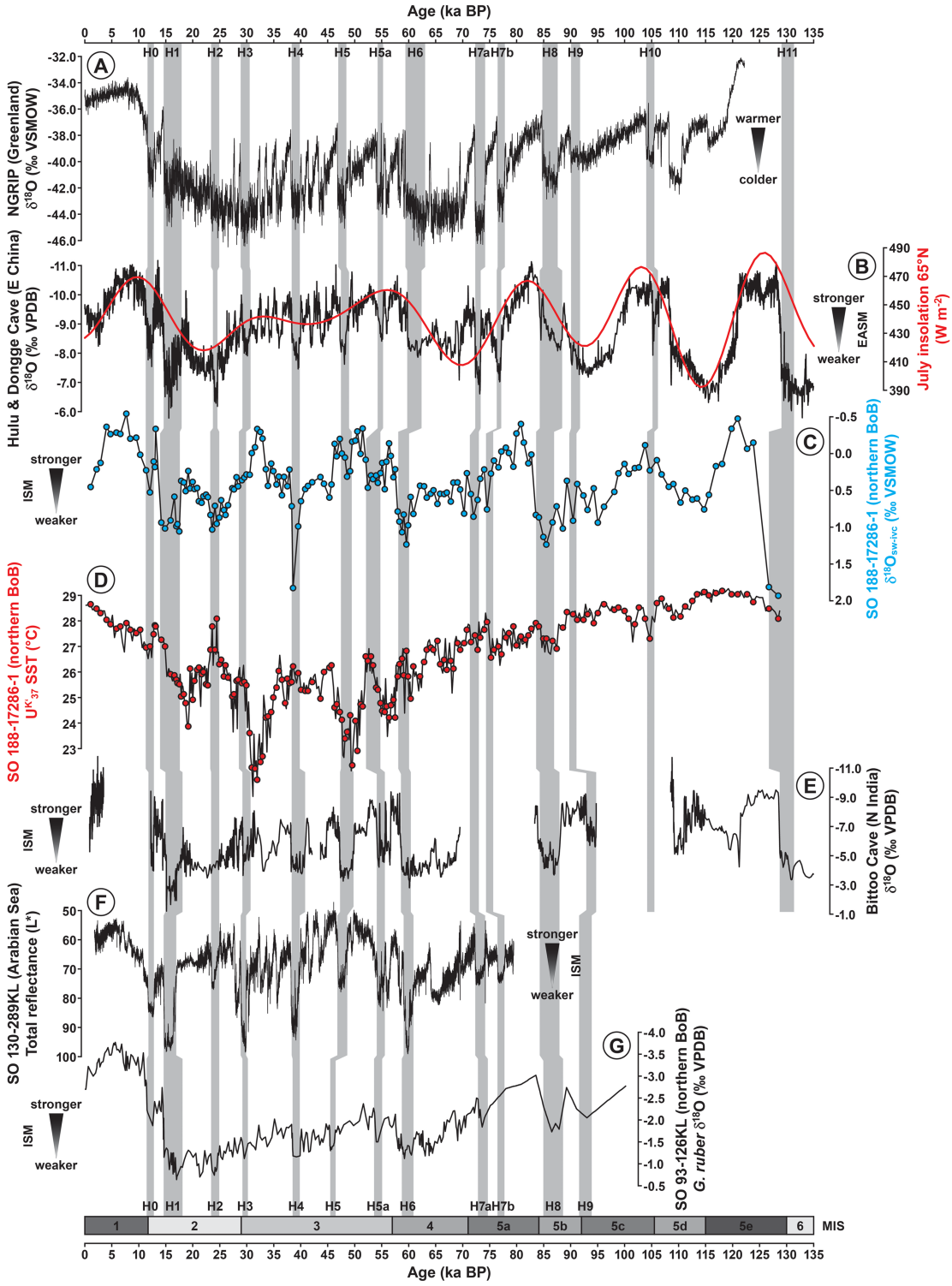

Figure 5. Comparison of proxy records of climatic changes in the North Atlantic realm and the ISM/EASM domain during the last ~130 kyr. (a) NGRIP ice core $\delta^{18}O$ record, Greenland (Seierstad et al., 2014), reflecting climate variability and particularly Heinrich events in the North Atlantic realm. (b) Combined $\delta^{18}O$ record of speleothems from Hulu and Dongge Cave, eastern China (Cheng et al., 2016), reflecting past EASM changes. (c and d) $\delta^{18}O_{sw\text{-}ivc}$ and $U^{K'}_{37}$-based SST records of Core 17286-1, northern BoB (this study). (e) Speleothem $\delta^{18}O$ record from Bittoo Cave, northern India (Kathayat et al., 2016), reflecting past ISM changes. (f) Spectral reflectance of Core SO 130-289KL, Arabian Sea (Deplazes et al., 2014), as a proxy for past ISM variability. (g) $\delta^{18}O$ of benthic foraminifera (*G. ruber*) from Core SO 93-126KL, northern BoB (Kudrass et al., 2001), as a proxy for past ISM variability. Marine isotope stages (MIS) are given for comparison with boundaries following Lisiecki and Raymo (2005) and Martín-Puertas et al. (2014). The gray bars mark Heinrich events (H0 (Younger Dryas) to H11) as reflected in the NGRIP ice core $\delta^{18}O$ record as well as their correlatives in the Asian monsoon proxy records.

values occurring at 106–90 and 83–73 ka BP, that is, during MIS 5c and 5a. From ~68 to ~15 ka BP, that is, during MIS 4 to MIS 2, $\delta^{18}O_{planktonic}$ ranges mainly between −2.0‰ and −1.0‰ but values of up to −0.5‰ are observed at 38–40 and 28–15 ka BP. A distinct drop in $\delta^{18}O_{planktonic}$ by ~1.5‰, starting at ~15 ka BP, characterizes the onset of MIS 1 (Figures 4 and 5).

After applying the corrections for changes in local SST and global ice volume (see section 3.4) to the measured $\delta^{18}O_{planktonic}$ values, the calculated $\delta^{18}O_{sw\text{-}ivc}$ reveals a characteristic multimillennial-scale variability. On the one hand, prominent episodes of low $\delta^{18}O_{sw\text{-}ivc}$ values occur at about 124–128, 108–98, 83–73, 57–46, and 33–31 ka BP, around 13 ka BP, and from ~10 to ~3 ka BP. On the other, also several short intervals of relatively higher $\delta^{18}O_{sw\text{-}ivc}$ values can be identified, which are superimposed on the multimillennial-scale variability. The most prominent of these short-term increases of $\delta^{18}O_{sw\text{-}ivc}$ are observed at 10.5–12.5, 13.5–18.0, 23.0–25.0, 38.0–40.5, 47.5–49.5, 52.0–55.0, and 58.0–60.5 ka BP, around 71.5–73.0 ka BP as well as at 74.0–76.0, 84.0–88.5, 89.5–91.0, 94.0–98.0, and 112.5–117.0 ka BP and before ~125.0 ka BP (Figures 4 and 5).

Although the $\delta^{18}O_{planktonic}$ record largely mirrors that of $\delta^{18}O_{benthic}$, there are also some distinct differences between the records. Most notable are occasional multimillennial offsets between distinct peaks in the $\delta^{18}O_{benthic}$ and $\delta^{18}O_{planctonic}$ records, for example, around 50–60 and 80–85 ka BP (Figure 4). A similar episodic out-of-phase behavior between $\delta^{18}O_{benthic}$ and $\delta^{18}O_{planctonic}$ has also been observed in other records from the Indian Ocean during the last glacial period (e.g., Dürkop et al., 2008; Jung et al., 2009) and is most likely a consequence of episodic propagations of Antarctic Intermediate Water (AAIW) into the northern Indian Ocean (cf. Ahmad et al., 2012; Jung et al., 2009; Yu et al., 2018). This could have influenced the oxygen isotope composition of the water in the intermediate Indian Ocean and consequently also $\delta^{18}O_{benthic}$, causing a temporal decoupling between the surface and deep water $\delta^{18}O$ signal. As the chronology of Core 17286-1 prior to ~40 ka BP is based on wiggle matching of the $\delta^{18}O_{benthic}$ record to the LS16 global $\delta^{18}O_{benthic}$ stack, an episodic influence of northward propagations of AAIW on $\delta^{18}O_{benthic}$ might have at least partly consequences for the age model and thus also for the relative timing of events in the $\delta^{18}O_{sw\text{-}ivc}$ record compared to other regional proxy records (see section 5.1 for further discussion).

5. Discussion

5.1. The $\delta^{18}O_{sw\text{-}ivc}$ Record and Evidence for Recurrent WMIs

To assess whether the Core 17286-1 $\delta^{18}O_{sw\text{-}ivc}$ record predominantly reflects ISM variability, it is first necessary to evaluate the reliability of the $U^{K'}_{37}$-based SST reconstruction as this is used to correct the measured $\delta^{18}O_{planktonic}$ values for the influence of superimposed SST changes.

In general, the $U^{K'}_{37}$ values obtained from Core 17286-1 are close to 1 (see section 4.2) and reconstructed SSTs should therefore be expected to be close to the upper end of the temperature range covered by global core top calibration studies, which is 28.5 to 30.0 °C (Conte et al., 2006;Müller et al., 1998 ; Sonzogni et al., 1997). As it has been shown that the relation between $U^{K'}_{37}$ and SST is not linear across the entire SST range but has a different slope above ~24 °C (e.g., Sonzogni et al., 1997; Tierney & Tingley, 2018), a calibration suitable for high $U^{K'}_{37}$ values and SSTs is necessary to get reliable temperature estimates for Core 17286-1. Therefore, a calibration equation established by Sonzogni et al. (1997) for the tropical and subtropical Indian Ocean for a temperature range of 24 to 29 °C has been chosen to convert the Core 17286-1 $U^{K'}_{37}$ values into SSTs (see section 3.3). In comparison to global core top calibrations (Müller et al., 1998; Sonzogni et al., 1997), which are linear over a much broader temperature range (0–30 °C), this yields a generally very similar trend throughout the record with all small-scale SST fluctuations being recorded, but generates more pronounced relative SST changes at the upper and lower end of the temperature range covered by the record, that is, above 28 °C and below 25 °C. Particularly, the more pronounced SST variability during MIS 5, which is also observed in other Indian Ocean SST records (Bard et al., 1997; Mohtadi et al., 2010; Saraswat et al., 2005; see discussion below), therefore clearly argues for applying a more temperature-confined calibration to the Core 17286-1 $U^{K'}_{37}$ data. However, it needs to be mentioned that reconstructed SSTs below 24 °C (e.g., around 30–35 and 50 ka BP) might be slightly too low as the applied calibration equation was developed only for the temperature range between 24 and 29 °C.

Furthermore, SSTs reconstructed from $U^{K'}_{37}$ might not necessarily reflect mean annual SST as initially proposed (Conte et al., 2006; Müller et al., 1998) but could possibly be seasonally biased towards the summer

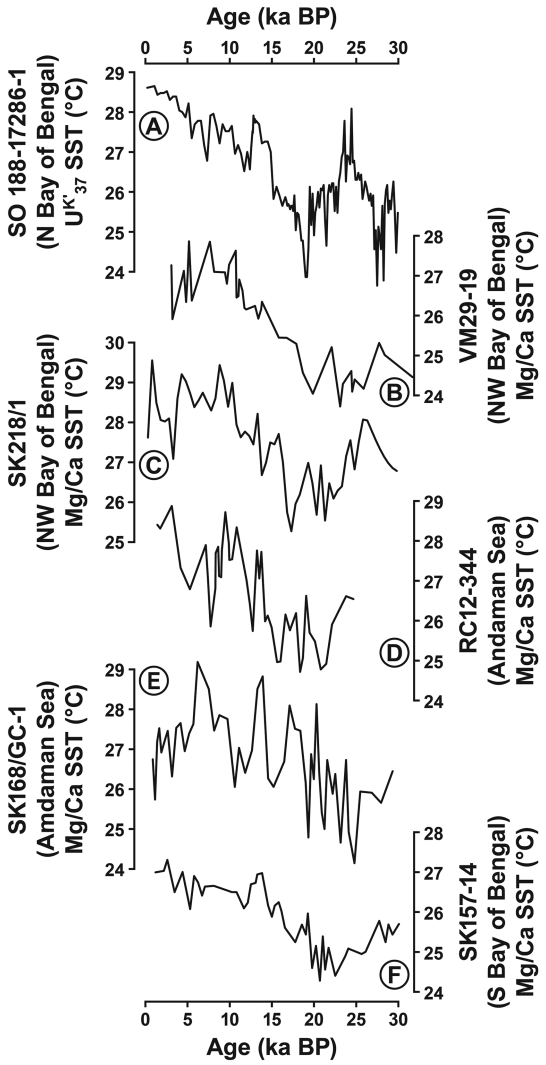

Figure 6. Comparison of SST records from the BoB and the Andaman Sea during the last ~30 kyr. (a) $U^{K'}_{37}$-based SST record of Core 17286-1, northern BoB (this study). (b) Mg/Ca-based SST record of Core VM29-19, northwestern BoB (Rashid et al., 2011). (c) Mg/Ca-based SST record of Core SK218/1, northwestern BoB (Govil & Naidu, 2011). (d) Mg/Ca-based SST record of Core RC12-344, Andaman Sea (Rashid et al., 2007). (e) Mg/Ca-based SST record of Core SK168/GC-1, Andaman Sea (Gebregiorgis et al., 2016). (f) Mg/Ca-based SST record of Core SK157-14, southern BoB (Raza et al., 2017). For the location of the individual proxy records see Figure 1b.

season as indicated by several studies utilizing for example sediment trap data and proxy-model comparisons (Schneider et al., 2010; Sonzogni et al., 1997; Wang et al., 2013). Nevertheless, despite the relatively complex seasonal cycle of coccolithiphore productivity in the Indian Ocean with the highest flux occurring during the summer monsoon season (Sonzogni et al., 1997), it has been shown that the productivity-weighted $U^{K'}_{37}$-SST relationship can be simply approximated by mean annual SST (Sonzogni et al., 1997), and therefore, the calibration equation applied to Core 17286-1 provides a reasonable measure for past mean annual SST variability in the northern BoB.

In support of our SST reconstruction, we find a generally good agreement of the Core 17286-1 $U^{K'}_{37}$-based SST record with foraminifera Mg/Ca-based SST reconstructions from the northern BoB and the adjacent Andaman Sea throughout the last ~30 kyr (Figure 6). These records indicate spatially largely consistent average SSTs, which varied between ~25.0 and ~27.0 °C during the LGM (20–26 ka BP) and between ~27.0 and ~29.0 °C during the Holocene (0–10 ka BP), consistently indicating an ocean surface warming of ~1.0–2.0 °C across Termination I (Gebregiorgis et al., 2016; Govil & Naidu, 2011; Rashid et al., 2007; Rashid et al., 2011; Raza et al., 2017). This is comparable to the $U^{K'}_{37}$-derived SST values recorded in Core 17286-1 (Figure 6). Although the foraminifera Mg/Ca-based SST reconstructions are characterized by a much higher short-term variability, particularly those from the northwestern BoB share several common features with the Core 17286-1 SST record, for example, slightly higher SSTs before the LGM and a continuous SST rise starting between 15 and 20 ka BP (Figure 6). In contrast, there are obvious differences between the BoB and Andaman Sea SST records, which might be related to oceanographic differences between both areas but can also be explained by chronological uncertainties as the chronologies of all other SST records displayed in Figure 6 are based on very simple age modeling approaches (linear interpolation between the uncertainty range midpoints of individual ^{14}C dates) and outdated ^{14}C calibration data sets.

In addition to the similarities between the Core 17286-1 SST reconstruction and adjacent SST records across Termination I, we also find a good overall agreement with long-term SST reconstructions from the equatorial Indian Ocean, particularly regarding the amplitude of SST changes. For example, a foraminifera Mg/Ca-based SST record off SW India (Core SK157/4; Figure 1a) also reveals slightly lower SSTs during the Holocene (~28.3 °C; 0–10 ka BP) than during MIS 5e (~28.6 °C; 115–130 ka BP) and a similar difference of ~1.3 °C between LGM (20–26 ka BP) and Holocene mean SST values (Saraswat et al., 2005). Also, the magnitude of SST variability throughout MIS 5 in this record, which is ~3.1 °C (~26.8 to ~29.9 °C; 71–130 ka BP), is comparable to the values in Core 17286-1 (~26.3 to ~29.3 °C; Figures 4 and 5). Lower SSTs during the Holocene (~27.3 °C) than during MIS 5e (~28.1 °C) and a SST variability of ~3.1 °C throughout MIS 5 (~25.6 to ~28.5 °C) are also revealed by a $U^{K'}_{37}$-based SST reconstruction from the eastern tropical Indian Ocean off SW Sumatra (Core GeoB 10038-41), although the SST rise from the LGM to the Holocene (~0.8 °C) appears slightly subdued there (Mohtadi et al., 2010). The relatively lower absolute SSTs in this record during MIS 5e compared to Core 17286-1 are, however, solely related to a different temperature calibration as the range of $U^{K'}_{37}$ values in both records is virtually identical (approximately 0.96 to 0.99). In addition, a foraminifera Mg/Ca-based SST reconstruction from the same site provides similar evidence for lower SSTs during the Holocene (~24.5 °C) than during MIS 5e (~25.5 °C), a deglacial SST rise of ~1.4 °C and a SST variability of ~3.2 °C throughout MIS 5 (~23.4 to ~26.6 °C), although reconstructed SST values are lower than for the $U^{K'}_{37}$-based reconstruction (Mohtadi et al., 2010). Furthermore, a low-resolution $U^{K'}_{37}$-based SST record

from Core MD90-963 off SW India (Figure 1a; Rostek et al., 1993) reveals a comparable LGM-Holocene SST difference of ~1.1 °C, but slightly higher instead of lower SSTs during the Holocene (~28.0 °C) compared to MIS 5e (~27.4 °C) and a rather subdued SST variability during MIS 5, which, however, might be attributed to the low temporal resolution of this record and the applied $U^{K'}_{37}$-SST calibration.

In summary, taking the good agreement with other regional SST records together with the fact that the reconstructed SST for the most recent sediments of Core 17286-1 is very close (within the uncertainty of the calibration) to the instrumentally recorded present-day mean annual SST at the coring site (see section 2), we are confident that the $U^{K'}_{37}$-based SST reconstruction for Core 17286-1 reliably reflects mean annual SST variability during the last ~130 kyr and can therefore be used to calculate $\delta^{18}O_{sw}$ from $\delta^{18}O_{planktonic}$. Nevertheless, it needs to be mentioned that $U^{K'}_{37}$ values during MIS 5e are mostly >0.98, that is, at the upper end of the calibration range, which is why reconstructed SSTs during this interval should be considered with caution with respect to the absolute values.

In consequence, the SST- and ice volume-corrected $\delta^{18}O_{sw\text{-}ivc}$ record can be considered to primarily reflect changes in ISM intensity throughout the last glacial-interglacial cycle. This is mainly related to the predominant influence of ^{18}O-depleted riverine freshwater from monsoon precipitation on the isotopic composition of the ocean surface water in the northern BoB in which the planktonic foraminifera grow. In particular, high freshwater input from the GBM river system during phases of strong ISM is lowering $\delta^{18}O_{sw\text{-}ivc}$ values whereas more positive values are indicative of less freshwater input and thus reduced ISM intensity. Although certain differences between $\delta^{18}O$ paleomonsoon records from the ISM and EASM domain, particularly regarding the magnitude of glacial-interglacial $\delta^{18}O$ variability, have recently been discussed (Cai et al., 2015), the Core 17286-1 $\delta^{18}O_{sw\text{-}ivc}$ data show in general a good agreement with EASM variability recorded in speleothems from Hulu and Dongge Cave in eastern China (Cheng et al., 2016; Figure 5). Moreover, not only long-term ISM changes throughout the last ~130 kyr are reflected in the Core 17286-1 $\delta^{18}O_{sw\text{-}ivc}$ record but also the short-term variability. Most prominent are several distinct, centennial- to millennial-scale episodes of relatively high $\delta^{18}O_{sw\text{-}ivc}$ values (see section 4.3), which are considered to reflect low riverine freshwater discharge and therefore particularly dry conditions in the ISM domain. These WMIs are characterized by a close synchroneity (within the uncertainty range of the Core 17286-1 chronology) with reductions in EASM intensity observed in speleothem $\delta^{18}O$ records from Hulu and Dongge Cave, eastern China (e.g., Cheng et al., 2016; Wang et al., 2001) as well as in ISM intensity recorded in speleothem $\delta^{18}O$ data from Bittoo Cave, northern India (Kathayat et al., 2016), and marine proxy records from the western Arabian Sea (Core SO 130-289KL; Deplazes et al., 2014) and the northern BoB (Core SO 93-126KL; Kudrass et al., 2001) (Figure 5). Slight differences between the Core 17286-1 $\delta^{18}O_{sw\text{-}ivc}$ and the Hulu and Dongge Cave $\delta^{18}O$ record, particularly regarding the overall shape and timing of individual events, for example, at the onset of MIS 5 or between ~50 and ~80 ka BP, are most likely related to (1) general differences between ISM and EASM paleomonsoon records due to differing changes in atmospheric circulation and moisture trajectories (cf. Cai et al., 2015), (2) the fact that the Core 17286-1 $\delta^{18}O_{sw\text{-}ivc}$ record indirectly reflects variability of ISM precipitation runoff through changes in BoB surface water conditions, while the Chinese stalagmites directly reflect changes in EASM precipitation amount, and (3) the inherent chronological uncertainty of the Core 17286-1 sediment record due to a variable and poorly assessed marine ^{14}C reservoir age (cf. Sarnthein et al., 2015), the uncertainty of the astronomical tuning of the $\delta^{18}O_{benthic}$ data, and the possible effect of episodic northward propagations of AAIW on the $\delta^{18}O_{benthic}$ record (see section 4.3). Particularly, the latter might explain the slight temporal offset observed for WMIs in the Core 17286-1 $\delta^{18}O_{sw\text{-}ivc}$ and the Hulu and Dongge Cave $\delta^{18}O$ record during the interval ~50–85 ka BP, which is, however, still within the range of the chronological uncertainty. Nevertheless, because of the generally good temporal agreement of WMI occurrence in the individual ISM and EASM proxy records, we conclude that WMIs are an overarching, synchronously occurring characteristic of the entire Asian monsoon system. We also observe a close temporal correspondence between WMIs and abrupt short-term shifts to colder temperatures during Heinrich events in the North Atlantic realm, which are most prominently recorded in the NGRIP ice core from Greenland (Rasmussen et al., 2014; Seierstad et al., 2014) (Figure 5). The most prominent reductions in monsoon precipitation around the northern BoB, inferred from pronounced positive peaks in the Core 17286-1 $\delta^{18}O_{sw\text{-}ivc}$ record, occurred during the Younger Dryas/Greenland Stadial 1 (sometimes referred to as

Heinrich event H0) as well as during Heinrich events H1, H2, H4, H5, H5a, H6, H7a, H7b, H8, H9, and H11. In contrast, the reduction in monsoon intensity during Heinrich events H3 and H10 was most probably rather weak as reflected by relatively small positive peaks in the $\delta^{18}O_{sw\text{-}ivc}$ record (Figure 5). The synchroneity between WMIs and Heinrich events throughout the last glacial period has previously been observed in several other paleomonsoon records (e.g., Cheng et al., 2016; Colin et al., 1998; Deplazes et al., 2014; Kathayat et al., 2016; Mingram et al., 2018; Mohtadi et al., 2014; Stager et al., 2011; Wang et al., 2001) and recently been proven by connecting Greenland ice core and Asian speleothem chronologies via cosmogenic radionuclides (Adolphi et al., 2018). However, although WMIs can therefore be considered as the regional Asian response to cold spells in the North Atlantic realm, the teleconnective mechanism that links the two regions is still debated.

5.2. Were WMIs Always Connected to Indian Ocean Surface Water Cooling Throughout the Last Glacial-Interglacial Cycle?

Several possible mechanisms have so far been considered to explain the observed close synchroneity between the occurrence of Heinrich events in the North Atlantic realm and WMIs in Asia and thus the climatic coupling between both regions. For example, it has been proposed that ISM weakening during North Atlantic cold spells was caused by perturbations of the subtropical westerly jet over Africa and Eurasia, driven by SST anomalies in the tropical Atlantic Ocean in response to freshwater input into the North Atlantic and related weakening of the Atlantic meridional overturning circulation (Marzin et al., 2013). Other studies instead suggest a reorganization of the Hadley circulation after the slowdown of the Atlantic meridional overturning circulation during Heinrich events, causing a southward displacement and parallel weakening of the Intertropical Convergence Zone (ITCZ) and finally a reduction of monsoon precipitation in Asia (Mohtadi et al., 2014). A similar repositioning of the ITCZ has also been favored as the most likely trigger for phases of reduced EASM strength in southeastern China during the Holocene (Yancheva et al., 2007). However, it needs to be mentioned in this context that for the weakening of the monsoon the reduction of the evaporative moisture content of the ITCZ is considered much more important than its repositioning (Stager et al., 2011). Furthermore, climate model simulations have also shown that reduced SSTs in the Indian Ocean in response to the cooling of the Northern Hemisphere (triggered by increasing sea ice extent in the North Atlantic), which are expected to reduce the evaporative moisture content of the ITCZ (cf. Stager et al., 2011), could possibly act as the link between Heinrich events and reduced monsoon intensity in Asia (Pausata et al., 2011). Particularly, the latter hypothesis of Indian Ocean SST lowering being the linking element between North Atlantic cold events and reductions in ISM intensity has recently been supported by evidence for ocean surface cooling during WMIs in the Arabian Sea derived from combining proxy data and climate modeling (Tierney et al., 2016). However, as the underlying foraminifera Mg/Ca- and $U^{K'}_{37}$-based SST reconstructions are not unambiguous and this linkage has only been established for the two most recent North Atlantic cold spells, that is, the Younger Dryas and Heinrich event H1, it is still unresolved whether this mechanism is also valid under full glacial boundary conditions. In this regard, longer marine proxy records from the Asian monsoon domain with paired $\delta^{18}O_{planktonic}/\delta^{18}O_{sw\text{-}ivc}$ and SST data could provide the opportunity to further test the relationship between Indian Ocean SST variability and changes in monsoon precipitation. Although there are already quite many paired $\delta^{18}O_{planktonic}$ and SST records from the northern Indian Ocean available (e.g., Anand et al., 2008; Gebregiorgis et al., 2016; Govil & Naidu, 2011; Kudrass et al., 2001; Rashid et al., 2007; Rashid et al., 2011; Saraswat et al., 2013; Tierney et al., 2016), most of them are rather short, mainly focusing on the last glacial-interglacial transition and rarely reaching beyond ~50 ka BP. In contrast, the only parallel $\delta^{18}O_{planktonic}$ and SST records that cover the entire last glacial-interglacial cycle are located in the equatorial Indian Ocean off SW India (Rostek et al., 1993; Saraswat et al., 2005) and off SW Sumatra (Mohtadi et al., 2010), which is rather outside the core zone of the ISM. As most of the mentioned records moreover lack the necessary temporal resolution to resolve centennial- to millennial-scale SST changes, it still remains ambiguous whether the proposed linkage between North Atlantic Heinrich events and WMIs via Indian Ocean SST changes (Pausata et al., 2011; Tierney et al., 2016) also prevails under different climatic boundary conditions throughout the entire last glacial period. The $U^{K'}_{37}$-based SST record derived from Core 17286-1 therefore offers, in conjunction with the parallel $\delta^{18}O_{sw\text{-}ivc}$ record, the opportunity to assess this relationship in more detail.

Comparing the SST record with the parallel $\delta^{18}O_{sw\text{-}ivc}$ data reveals that WMIs were apparently only in very few cases accompanied by decreases in SST (Figures 4 and 5). In particular, we observe a correspondence between reduced ISM intensity and lower SSTs in the BoB only for the two most recent intervals of reduced monsoon precipitation, which occurred parallel to the Younger Dryas and Heinrich event H1, but even in these cases the decreases in SST are not very pronounced. An exception might be the WMI that parallels Heinrich event H5, which, however, occurred during a longer phase of relatively low Indian Ocean SST (Figure 5), thus questioning a direct relationship at submillennial time scales. Hence, although our observation of slightly reduced SSTs during the two most recent WMIs is in agreement with the findings of Tierney et al. (2016), the apparent lack of pronounced SST decreases during WMIs that occurred under glacial boundary conditions, that is, before ~15 ka BP, and even during Termination II clearly challenges the general validity of a direct connection between lowered SSTs in the Indian Ocean and reduced monsoon precipitation as proposed by Pausata et al. (2011) and Tierney et al. (2016). In fact, we observe only very subdued SST changes during most of the WMIs and in some cases even temporarily increased SSTs, for example, for the WMIs that correspond to Heinrich Events H2, H3, H4, H5a, and H6 (Figure 5). We also find no evidence for a mediation of the parallel occurrence of WMIs and Indian Ocean SST changes through the superimposition of changes in the Earth's orbital parameters, that is, a parallel occurrence of SST reductions and WMIs during either maxima or minima in Northern Hemisphere insolation. This is in good agreement with findings from mainland NE China, indicating that phases of EASM weakening occurred synchronously to Heinrich events regardless the insolation forcing (Mingram et al., 2018). Hence, the assumption that WMIs are in general coupled to North Atlantic Heinrich events via cooling of the Indian Ocean surface water must at least be questioned based on the proxy evidence from Core 17286-1. Although our data do not provide information about possible SST changes and their relation to WMIs in the source region of the ISM, that is, the western Indian Ocean, our interpretation is supported by other proxy records from the Arabian Sea (Anand et al., 2008; Saher et al., 2007; Saraswat et al., 2013) and the BoB (Panmei et al., 2017), which show no particular cooling of the Indian Ocean surface water during the most recent WMIs, occurring contemporaneously to the Younger Dryas and Heinrich events H1 and H2 in the North Atlantic realm. Furthermore, the general validity of Indian Ocean SST lowering being the trigger of WMIs is also questioned by compelling evidence from combined climate modeling and examination of instrumental data, showing that the weakening of the ISM during the last decades is paralleled by Indian Ocean warming rather than by cooling (Roxy et al., 2015). Hence, the connection between SST changes in the Indian Ocean and the occurrence of WMIs is apparently more complex than initially suggested with probably significant spatial and temporal differences between (1) the BoB and the Arabian Sea and (2) post-LGM and full glacial climatic boundary conditions. A more complex, transient triggering of WMIs in the Asian monsoon domain would be in line with a previous study, suggesting that short-term EASM variability during the deglaciation was mainly controlled by processes in the Northern Hemisphere while during the last glacial period the influence of Southern Hemisphere climate variability prevailed (Rohling et al., 2009). Furthermore, other mechanisms such as the proposed perturbation of the subtropical westerly jet over Africa and Eurasia (Marzin et al., 2013) or a reorganization of the Hadley circulation and an associated displacement of the ITCZ (Mohtadi et al., 2014) should also be considered to explain the teleconnective coupling between Heinrich events and WMIs. Particularly, the latter mechanism is corroborated by speleothem $\delta^{18}O$ data from Ball Gown Cave, northern Australia (Denniston et al., 2013), pollen data from Lynch's Crater, northern Australia (Muller et al., 2008), and speleothem $\delta^{18}O$ data from Liang Luar Cave, south-central Indonesia (Ayliffe et al., 2013), which are all located south of the present-day mean position of the ITCZ. These records provide evidence for increased precipitation during Heinrich events, most likely reflecting a southward displacement of the ITCZ. This would be in line with a synchronous reduction of monsoon precipitation in the northern BoB and other paleomonsoon records north of the equator, reflecting a hemispheric antiphased pattern of ITCZ-controlled monsoon changes. However, such shifts in the position of the ITCZ, if supposed to be of a considerable latitudinal range, were most likely rather limited in their longitudinal extent (McGee et al., 2014). In consequence, further studies are necessary to finally clarify the linkage between North Atlantic Heinrich events and WMIs in Asia and to shed light on the possible influence of Southern Hemisphere climate variability. This should particularly include the establishment of new paired high-resolution SST and $\delta^{18}O_{sw\text{-}ivc}$ records from the source region of the ISM, the Arabian Sea, to clarify the relationship between SST changes and WMIs in this region also under full glacial climatic boundary conditions.

6. Conclusions

Paired foraminifera $\delta^{18}O$ and $U^{K'}_{37}$-based SST data obtained from Core 17286-1 represent the first records of paleoceanographic changes in the northern BoB that cover the entire last glacial-interglacial cycle at submillennial-scale resolution. The $\delta^{18}O_{planktonic}$ record provides clear evidence for changes in Indian Ocean surface water conditions in response to variable riverine freshwater input due to changing ISM intensity. Orbital- to millennial-scale changes in ISM intensity thereby reveal a good temporal agreement with other regional paleomonsoon records but also with proxy data from the EASM domain. Furthermore, several short-term reductions of ISM intensity are documented for the first time throughout the last glacial period in this part of the Indian Ocean. These WMIs occurred synchronously to similar events previously documented in other terrestrial and marine paleomonsoon archives, but also to cold Heinrich events in the North Atlantic realm. However, when compared with the parallel $U^{K'}_{37}$-based SST record, which is so far the first regional high-resolution data set of this kind that covers the entire last glacial-interglacial cycle, we find only in very rare cases a correspondence between SST reductions and WMIs recorded in the $\delta^{18}O_{planktonic}/\delta^{18}O_{sw\text{-}ivc}$ record. This challenges the previous assumption that Indian Ocean SST represents the linking element between cold Heinrich events in the North Atlantic realm and WMIs in the ISM domain. Hence, other mechanisms must be invoked to explain the evident synchroneity of climatic events between these two regions.

Acknowledgments
We thank the crew and captain of R/V *Sonne* and the scientific staff of Cruise SO 188 for core recovery. This work was supported by the German Research Association (DFG) within the frame of Priority Programme SPP 1266—*Integrated Analysis of Interglacial Climate Dynamics* (Grant 207008408). The work of S. Lauterbach was funded through a grant to R. R. Schneider within the frame of DFG Priority Programme SPP 527—*International Ocean Discovery Programme* (Grant 387728878). We thank the colleagues of the Radiometric Dating working group at the Leibniz Laboratory for AMS ^{14}C dating; S. Koch for alkenone measurements; N. Tate, S. Lüders, and I. Thate for their assistance with sediment processing and foraminifera picking; and K. Gramenz and P. Schindler for stable isotope analyses. The valuable comments of two anonymous reviewers greatly helped to improve the manuscript. All proxy data obtained from Core SO 188-17286-1 are available via the World Data Center PANGAEA (www.pangaea.de).

References

Adolphi, F., Bronk Ramsey, C., Erhardt, T., Edwards, R. L., Cheng, H., Turney, C. S. M., et al. (2018). Connecting the Greenland ice-core and UTh timescales via cosmogenic radionuclides: Testing the synchroneity of Dansgaard–Oeschger events. *Climate of the Past*, *14*(11), 1755–1781. https://doi.org/10.5194/cp-14-1755-2018

Ahmad, S. M., Zheng, H., Raza, W., Zhou, B., Lone, M. A., Raza, T., & Suseela, G. (2012). Glacial to Holocene changes in the surface and deep waters of the northeast Indian Ocean. *Marine Geology*, *329–331*, 16–23. https://doi.org/10.1016/j.margeo.2012.10.002

Anand, P., Kroon, D., Singh Arun, D., Ganeshram Raja, S., Ganssen, G., & Elderfield, H. (2008). Coupled sea surface temperature–seawater $\delta^{18}O$ reconstructions in the Arabian Sea at the millennial scale for the last 35 ka. *Paleoceanography*, *23*, PA4207. https://doi.org/10.1029/2007PA001564

Ayliffe, L. K., Gagan, M. K., Zhao, J.-X., Drysdale, R. N., Hellstrom, J. C., Hantoro, W. S., et al. (2013). Rapid interhemispheric climate links via the Australasian monsoon during the last deglaciation. *Nature Communications*, *4*, 2908. https://doi.org/10.1038/ncomms3908

Bard, E., Rostek, F., & Sonzogni, C. (1997). Interhemispheric synchrony of the last deglaciation inferred from alkenone palaeothermometry. *Nature*, *385*, 707–710. https://doi.org/10.1038/385707a0

Bemis, B. E., Spero, H. J., Bijma, J., & Lea, D. W. (1998). Reevaluation of the oxygen isotopic composition of planktonic foraminifera: Experimental results and revised paleotemperature equations. *Paleoceanography*, *13*, 150–160. https://doi.org/10.1029/98PA00070

Bolton, C. T., Chang, L., Clemens, S. C., Kodama, K., Ikehara, M., Medina-Elizalde, M., et al. (2013). A 500,000 year record of Indian summer monsoon dynamics recorded by eastern equatorial Indian Ocean upper water-column structure. *Quaternary Science Reviews*, *77*, 167–180. https://doi.org/10.1016/j.quascirev.2013.07.031

Boyer, T. P., Antonov, J. I., Baranova, O. K., Coleman, C., Garcia, H. E., Grodsky, A., et al. (2013). World ocean database 2013. in NOAA Atlas NESDIS 72, p. 209, Silver Spring, MD.

Brassell, S. C., Eglinton, G., Marlowe, I. T., Pflaumann, U., & Sarnthein, M. (1986). Molecular stratigraphy: A new tool for climatic assessment. *Nature*, *320*, 129–133. https://doi.org/10.1038/320129a0

Bronk Ramsey, C. (2008). Deposition models for chronological records. *Quaternary Science Reviews*, *27*, 42–60. https://doi.org/10.1016/j.quascirev.2007.01.019

Bronk Ramsey, C. (2009a). Bayesian analysis of radiocarbon dates. *Radiocarbon*, *51*, 337–360. https://doi.org/10.1017/S0033822200033865

Bronk Ramsey, C. (2009b). Dealing with outliers and offsets in radiocarbon dating. *Radiocarbon*, *51*, 1023–1045. https://doi.org/10.1017/S0033822200034093

Bronk Ramsey, C., & Lee, S. (2013). Recent and planned developments of the program OxCal. *Radiocarbon*, *55*, 720–730. https://doi.org/10.1017/S0033822200057878

Cai, Y., Fung, I. Y., Edwards, R. L., An, Z., Cheng, H., Lee, J. E., et al. (2015). Variability of stalagmite-inferred Indian monsoon precipitation over the past 252,000 y. *Proceedings of the National Academy of Sciences of the United States of America*, *112*(10), 2954–2959. https://doi.org/10.1073/pnas.1424035112

Caley, T., Malaizé, B., Zaragosi, S., Rossignol, L., Bourget, J., Eynaud, F., et al. (2011). New Arabian Sea records help decipher orbital timing of Indo-Asian monsoon. *Earth and Planetary Science Letters*, *308*(3-4), 433–444. https://doi.org/10.1016/j.epsl.2011.06.019

Caley, T., Roche, D. M., & Renssen, H. (2014). Orbital Asian summer monsoon dynamics revealed using an isotope-enabled global climate model. *Nature Communications*, *5*, 5371. https://doi.org/10.1038/ncomms6371

Cheng, H., Edwards, R. L., Sinha, A., Spötl, C., Yi, L., Chen, S., et al. (2016). The Asian monsoon over the past 640,000 years and ice age terminations. *Nature*, *534*(7609), 640–646. https://doi.org/10.1038/nature18591

Clemens, S. C., & Prell, W. L. (2003). A 350,000 year summer-monsoon multi-proxy stack from the Owen Ridge, Northern Arabian Sea. *Marine Geology*, *201*, 35–51. https://doi.org/10.1016/S0025-3227(03)00207-X

Clemens, S. C., Prell, W. L., & Sun, Y. B. (2010). Orbital-scale timing and mechanisms driving Late Pleistocene Indo-Asian summer monsoons: Reinterpreting cave speleothem $\delta^{18}O$. *Paleoceanography*, *25*, PA4207. https://doi.org/10.1029/2010PA001926

Colin, C., Kissel, C., Blamart, D., & Turpin, L. (1998). Magnetic properties of sediments in the Bay of Bengal and the Andaman Sea: Impact of rapid North Atlantic Ocean climatic events on the strength of the Indian monsoon. *Earth and Planetary Science Letters*, *160*, 623–635. https://doi.org/10.1016/S0012-821X(98)00116-2

Conte, M. H., Sicre, M. A., Rühlemann, C., Weber, J. C., Schulte, S., Schulz-Bull, D., & Blanz, T. (2006). Global temperature calibration of the alkenone unsaturation index ($U^{K'}_{37}$) in surface waters and comparison with surface sediments. *Geochemistry, Geophysics, Geosystems*, *7*, Q02005. https://doi.org/10.1029/2005GC001054

Contreras-Rosales, L. A., Jennerjahn, T., Tharammal, T., Meyer, V., Lückge, A., Paul, A., & Schefuß, E. (2014). Evolution of the Indian Summer Monsoon and terrestrial vegetation in the Bengal region during the past 18 ka. *Quaternary Science Reviews*, *102*, 133–148. https://doi.org/10.1016/j.quascirev.2014.08.010

Delaygue, G., Bard, E., Rollion, C., Jouzel, J., Stiévenard, M., Duplessy, J. C., & Ganssen, G. (2001). Oxygen isotope/salinity relationship in the northern Indian Ocean. *Journal of Geophysical Research*, *106*, 4565–4574. https://doi.org/10.1029/1999JC000061

Denniston, R. F., Wyrwoll, K. H., Asmerom, Y., Polyak, V. J., Humphreys, W. F., Cugley, J., et al. (2013). North Atlantic forcing of millennial-scale Indo-Australian monsoon dynamics during the Last Glacial period. *Quaternary Science Reviews*, *72*, 159–168. https://doi.org/10.1016/j.quascirev.2013.04.012

Deplazes, G., Lückge, A., Peterson, L. C., Timmermann, A., Hamann, Y., Hughen, K. A., et al. (2013). Links between tropical rainfall and North Atlantic climate during the last glacial period. *Nature Geoscience*, *6*(3), 213–217. https://doi.org/10.1038/ngeo1712

Deplazes, G., Lückge, A., Stuut, J. B. W., Pätzold, J., Kuhlmann, H., Husson, D., et al. (2014). Weakening and strengthening of the Indian monsoon during Heinrich events and Dansgaard-Oeschger oscillations. *Paleoceanography*, *29*, 99–114. https://doi.org/10.1002/2013PA002509

Dürkop, A., Holbourn, A., Kuhnt, W., Zuraida, R., Andersen, N., & Grootes, P. M. (2008). Centennial-scale climate variability in the Timor Sea during Marine Isotope Stage 3. *Marine Micropaleontology*, *66*, 208–221. https://doi.org/10.1016/j.marmicro.2007.10.002

Etourneau, J., Schneider, R., Blanz, T., & Martinez, P. (2010). Intensification of the Walker and Hadley atmospheric circulations during the Pliocene–Pleistocene climate transition. *Earth and Planetary Science Letters*, *297*, 103–110. https://doi.org/10.1016/j.epsl.2010.06.010

Gadgil, S., & Rupa Kumar, K. (2006). The Asian monsoon—Agriculture and economy. In B. Wang (Ed.), *The Asian Monsoon*, (pp. 651–683). Berlin: Springer.

Gebregiorgis, D., Hathorne, E. C., Sijinkumar, A. V., Nath, B. N., Nürnberg, D., & Frank, M. (2016). South Asian summer monsoon variability during the last ~54 kyrs inferred from surface water salinity and river runoff proxies. *Quaternary Science Reviews*, *138*, 6–15. https://doi.org/10.1016/j.quascirev.2016.02.012

Govil, P., & Naidu, P. D. (2011). Variations of Indian monsoon precipitation during the last 32 kyr reflected in the surface hydrography of the Western Bay of Bengal. *Quaternary Science Reviews*, *30*, 3871–3879. https://doi.org/10.1016/j.quascirev.2011.10.004

Hijmans, R. J., Cameron, S. E., Parra, J. L., Jones, P. G., & Jarvis, A. (2005). Very high resolution interpolated climate surfaces for global land areas. *International Journal of Climatology*, *25*, 1965–1978. https://doi.org/10.1002/joc.1276

Huang, E., Chen, Y., Schefuß, E., Steinke, S., Liu, J., Tian, J., et al. (2018). Precession and glacial-cycle controls of monsoon precipitation isotope changes over East Asia during the Pleistocene. *Earth and Planetary Science Letters*, *494*, 1–11. https://doi.org/10.1016/j.epsl.2018.04.046

Jung, S. J. A., Kroon, D., Ganssen, G., Peeters, F., & Ganeshram, R. (2009). Enhanced Arabian Sea intermediate water flow during glacial North Atlantic cold phases. *Earth and Planetary Science Letters*, *280*, 220–228. https://doi.org/10.1016/j.epsl.2009.01.037

Kathayat, G., Cheng, H., Sinha, A., Spötl, C., Edwards, R. L., Zhang, H., et al. (2016). Indian monsoon variability on millennial-orbital timescales. *Scientific Reports*, *6*, 24374. https://doi.org/10.1038/srep24374

Kudrass, H. R., Hofmann, A., Doose, H., Emeis, K., & Erlenkeuser, H. (2001). Modulation and amplification of climatic changes in the Northern Hemisphere by the Indian summer monsoon during the past 80 k.y. *Geology*, *29*, 63–66. https://doi.org/10.1130/0091-7613(2001)029<0063:MAAOCC>2.0.CO;2

Lisiecki, L. E., & Raymo, M. E. (2005). A Pliocene-Pleistocene stack of 57 globally distributed benthic $\delta^{18}O$ records. *Paleoceanography*, *20*, PA1003. https://doi.org/10.1029/2004PA001071

Lisiecki, L. E., & Stern, J. V. (2016). Regional and global benthic $\delta^{18}O$ stacks for the last glacial cycle. *Paleoceanography*, *31*, 1368–1394. https://doi.org/10.1002/2016PA003002

Marlowe, I. T., Brassell, S. C., Eglinton, G., & Green, J. C. (1984). Long chain unsaturated ketones and esters in living algae and marine sediments. *Organic Geochemistry*, *6*, 135–141. https://doi.org/10.1016/0146-6380(84)90034-2

Marlowe, I. T., Brassell, S. C., Eglinton, G., & Green, J. C. (1990). Long-chain alkenones and alkyl alkenoates and the fossil coccolith record of marine sediments. *Chemical Geology*, *88*, 349–375. https://doi.org/10.1016/0009-2541(90)90098-R

Martín-Puertas, C., Brauer, A., Wulf, S., Ott, F., Lauterbach, S., & Dulski, P. (2014). Annual proxy data from Lago Grande di Monticchio (southern Italy) between 76 and 112 ka: New chronological constraints and insights on abrupt climatic oscillations. *Climate of the Past*, *10*, 2099–2114. https://doi.org/10.5194/cp-10-2099-2014

Marzin, C., Kallel, N., Kageyama, M., Duplessy, J. C., & Braconnot, P. (2013). Glacial fluctuations of the Indian monsoon and their relationship with North Atlantic climate: New data and modelling experiments. *Climate of the Past*, *9*, 2135–2151. https://doi.org/10.5194/cp-9-2135-2013

McGee, D., Donohoe, A., Marshall, J., & Ferreira, D. (2014). Changes in ITCZ location and cross-equatorial heat transport at the Last Glacial Maximum, Heinrich Stadial 1, and the mid-Holocene. *Earth and Planetary Science Letters*, *390*, 69–79. https://doi.org/10.1016/j.epsl.2013.12.043

Milliman, J. D., & Farnsworth, K. L. (2011). *River discharge to the Coastal Ocean: A global synthesis*. Cambridge: Cambridge University Press.

Mingram, J., Stebich, M., Schettler, G., Hu, Y., Rioual, P., Nowaczyk, N., et al. (2018). Millennial-scale East Asian monsoon variability of the last glacial deduced from annually laminated sediments from Lake Sihailongwan, N.E. China. *Quaternary Science Reviews*, *201*, 57–76. https://doi.org/10.1016/j.quascirev.2018.09.023

Mohtadi, M., Lückge, A., Steinke, S., Groeneveld, J., Hebbeln, D., & Westphal, N. (2010). Late Pleistocene surface and thermocline conditions of the eastern tropical Indian Ocean. *Quaternary Science Reviews*, *29*, 887–896. https://doi.org/10.1016/j.quascirev.2009.12.006

Mohtadi, M., Prange, M., Oppo, D. W., de Pol-Holz, R., Merkel, U., Zhang, X., et al. (2014). North Atlantic forcing of tropical Indian Ocean climate. *Nature*, *509*(7498), 76–80. https://doi.org/10.1038/nature13196

Muller, J., Kylander, M., Wüst, R. A. J., Weiss, D., Martinez-Cortizas, A., LeGrande, A. N., et al. (2008). Possible evidence for wet Heinrich phases in tropical NE Australia: The Lynch's Crater deposit. *Quaternary Science Reviews*, *27*(5-6), 468–475. https://doi.org/10.1016/j.quascirev.2007.11.006

Müller, P. J., Kirst, G., Ruhland, G., von Storch, I., & Rosell-Melé, A. (1998). Calibration of the alkenone paleotemperature index $U^{K'}_{37}$ based on core-tops from the eastern South Atlantic and the global ocean (60°N-60°S). *Geochimica et Cosmochimica Acta*, *62*, 1757–1772. https://doi.org/10.1016/S0016-7037(98)00097-0

Panmei, C., Divakar Naidu, P., & Mohtadi, M. (2017). Bay of Bengal exhibits warming trend during the Younger Dryas: Implications of AMOC. *Geochemistry, Geophysics, Geosystems*, *18*, 4317–4325. https://doi.org/10.1002/2017GC007075

Pausata, F. S. R., Battisti, D. S., Nisancioglu, K. H., & Bitz, C. M. (2011). Chinese stalagmite $\delta^{18}O$ controlled by changes in the Indian monsoon during a simulated Heinrich event. *Nature Geoscience*, *4*, 474–480. https://doi.org/10.1038/ngeo1169

Prahl, F. G., & Wakeham, S. G. (1987). Calibration of unsaturation patterns in long-chain ketone compositions for palaeotemperature assessment. *Nature*, *330*, 367–369. https://doi.org/10.1038/330367a0

Rashid, H., England, E., Thompson, L., & Polyak, L. (2011). Late Glacial to Holocene Indian Summer Monsoon Variability Based upon Sediment Records Taken from the Bay of Bengal. *Terrestrial, Atmospheric and Oceanic Sciences*, *22*, 215–228. https://doi.org/0.3319/TAO.2010.09.17.02(TibXS)

Rashid, H., Flower, B. P., Poore, R. Z., & Quinn, T. M. (2007). A ~ 25 ka Indian Ocean monsoon variability record from the Andaman Sea. *Quaternary Science Reviews*, *26*, 2586–2597. https://doi.org/10.1016/j.quascirev.2007.07.002

Rasmussen, S. O., Bigler, M., Blockley, S. P., Blunier, T., Buchardt, S. L., Clausen, H. B., et al. (2014). A stratigraphic framework for abrupt climatic changes during the Last Glacial period based on three synchronized Greenland ice-core records: Refining and extending the INTIMATE event stratigraphy. *Quaternary Science Reviews*, *106*, 14–28. https://doi.org/10.1016/j.quascirev.2014.09.007

Raza, T., Ahmad, S. M., Steinke, S., Raza, W., Lone, M. A., Beja, S. K., & Suseela, G. (2017). Glacial to Holocene changes in sea surface temperature and seawater $\delta^{18}O$ in the northern Indian Ocean. *Palaeogeography, Palaeoclimatology, Palaeoecology*, *485*, 697–705. https://doi.org/10.1016/j.palaeo.2017.07.026

Reimer, P. J., Bard, E., Bayliss, A., Beck, J. W., Blackwell, P. G., Ramsey, C. B., et al. (2013). IntCal13 and Marine13 radiocarbon age calibration curves 0–50,000 years cal BP. *Radiocarbon*, *55*(4), 1869–1887. https://doi.org/10.2458/azu_js_rc.55.16947

Rohde Krossa, V., Moros, M., Leduc, G., Hinz, M., Blanz, T., & Schneider, R. (2017). Regional climate change and the onset of farming in northern Germany and southern Scandinavia. *The Holocene*, *27*, 1589–1599. https://doi.org/10.1177/0959683617702223

Rohling, E. J., Liu, Q. S., Roberts, A. P., Stanford, J. D., Rasmussen, S. O., Langen, P. L., & Siddall, M. (2009). Controls on the East Asian monsoon during the last glacial cycle, based on comparison between Hulu Cave and polar ice-core records. *Quaternary Science Reviews*, *28*, 3291–3302. https://doi.org/10.1016/j.quascirev.2009.09.007

Rosell-Melé, A., Eglinton, G., Pflaumann, U., & Sarnthein, M. (1995). Atlantic core-top calibration of the U^{K}_{37} index as a sea-surface palaeotemperature indicator. *Geochimica et Cosmochimica Acta*, *59*, 3099–3107. https://doi.org/10.1016/0016-7037(95)00199-A

Rostek, F., Ruhlandt, G., Bassinot, F. C., Müller, P. J., Labeyrie, L. D., Lancelot, Y., & Bard, E. (1993). Reconstructing sea surface temperature and salinity using $\delta^{18}O$ and alkenone records. *Nature*, *364*, 319–321. https://doi.org/10.1038/364319a0

Roxy, M. K., Ritika, K., Terray, P., Murtugudde, R., Ashok, K., & Goswami, B. N. (2015). Drying of Indian subcontinent by rapid Indian Ocean warming and a weakening land-sea thermal gradient. *Nature Communications*, *6*, 7423. https://doi.org/10.1038/ncomms8423

Saher, M. H., Jung, S. J. A., Elderfield, H., Greaves, M. J., & Kroon, D. (2007). Sea surface temperatures of the western Arabian Sea during the last deglaciation. *Paleoceanography*, *22*, PA2208. https://doi.org/10.1029/2006pa001292

Saraswat, R., Lea, D. W., Nigam, R., Mackensen, A., & Naik, D. K. (2013). Deglaciation in the tropical Indian Ocean driven by interplay between the regional monsoon and global teleconnections. *Earth and Planetary Science Letters*, *375*, 166–175. https://doi.org/10.1016/j.epsl.2013.05.022

Saraswat, R., Nigam, R., Weldeab, S., Mackensen, A., & Naidu, P. D. (2005). A first look at past sea surface temperatures in the equatorial Indian Ocean from Mg/Ca in foraminifera. *Geophysical Research Letters*, *32*, L24605. https://doi.org/10.1029/2005GL024093

Sarnthein, M., Balmer, S., Grootes, P. M., & Mudelsee, M. (2015). Planktic and benthic ^{14}C reservoir ages for three ocean basins, calibrated by a suite of ^{14}C plateaus in the glacial-to-deglacial Suigetsu atmospheric ^{14}C record. *Radiocarbon*, *57*, 129–151. https://doi.org/10.2458/azu_rc.57.17916

Schneider, B., Leduc, G., & Park, W. (2010). Disentangling seasonal signals in Holocene climate trends by satellite-model-proxy integration. *Paleoceanography*, *25*, PA4217. https://doi.org/10.1029/2009pa001893

Schulz, H., von Rad, U., & Erlenkeuser, H. (1998). Correlation between Arabian Sea and Greenland climate oscillations of the past 110,000 years. *Nature*, *393*, 54–57. https://doi.org/10.1038/31750

Seierstad, I. K., Abbott, P. M., Bigler, M., Blunier, T., Bourne, A. J., Brook, E., et al. (2014). Consistently dated records from the Greenland GRIP, GISP2 and NGRIP ice cores for the past 104 ka reveal regional millennial-scale $\delta^{18}O$ gradients with possible Heinrich event imprint. *Quaternary Science Reviews*, *106*, 29–46. https://doi.org/10.1016/j.quascirev.2014.10.032

Sen Gupta, R., & Naqvi, S. W. A. (1984). Chemical oceanography of the Indian Ocean, north of the equator. *Deep Sea Research Part A. Oceanographic Research Papers*, *31*, 671–706. https://doi.org/10.1016/0198-0149(84)90035-9

Sengupta, S., Parekh, A., Chakraborty, S., Ravi Kumar, K., & Bose, T. (2013). Vertical variation of oxygen isotope in Bay of Bengal and its relationships with water masses. *Journal of Geophysical Research: Oceans*, *118*, 6411–6424. https://doi.org/10.1002/2013JC008973

Sijinkumar, A. V., Clemens, S., Nath, B. N., Prell, W., Benshila, R., & Lengaigne, M. (2016). $\delta^{18}O$ and salinity variability from the Last Glacial Maximum to recent in the Bay of Bengal and Andaman Sea. *Quaternary Science Reviews*, *135*, 79–91. https://doi.org/10.1016/j.quascirev.2016.01.022

Singh, A., Jani, R. A., & Ramesh, R. (2010). Spatiotemporal variations of the $\delta^{18}O$–salinity relation in the northern Indian Ocean. *Deep Sea Research Part I: Oceanographic Research Papers*, *57*, 1422–1431. https://doi.org/10.1016/j.dsr.2010.08.002

Sonzogni, C., Bard, E., Rostek, F., Dollfus, D., Rosell-Melé, A., & Eglinton, G. (1997). Temperature and salinity effects on alkenone ratios measured in surface sediments from the Indian Ocean. *Quaternary Research*, *47*, 344–355. https://doi.org/10.1006/qres.1997.1885

Southon, J., Kashgarian, M., Fontugne, M., Metivier, B., & Yim, W. W. S. (2002). Marine reservoir corrections for the Indian Ocean and southeast Asia. *Radiocarbon*, *44*, 167–180. https://doi.org/10.1017/S0033822200064778

Spieß, V., Schwenk, T., Bartels, T., Blanz, T., Etourneau, J., Gainusa-Bogdan, A., et al. (2006). Cruise Report SO 188-1 (*Bengal Sea Level*, FS Sonne, Singapore (Singapore)—Chittagong (Bangladesh), 06.06.2006 – 04.07.2006), 72 pp., Universität Bremen, Fachbereich Geowissenschaften, Bremen. https://doi.org/10.2312/cr_so188_1

Stager, J. C., Ryves, D. B., Chase, B. M., & Pausata, F. S. R. (2011). Catastrophic drought in the Afro-Asian monsoon region during Heinrich Event 1. *Science*, *331*(6022), 1299–1302. https://doi.org/10.1126/science.1198322

Thomas, E. K., Clemens, S. C., Prell, W. L., Herbert, T. D., Huang, Y., Liu, Z., et al. (2014). Temperature and leaf wax $\delta^{2}H$ records demonstrate seasonal and regional controls on Asian monsoon proxies. *Geology*, *42*(12), 1075–1078. https://doi.org/10.1130/G36289.1

Tierney, J. E., Pausata, F. S. R., & deMenocal, P. (2016). Deglacial Indian monsoon failure and North Atlantic stadials linked by Indian Ocean surface cooling. *Nature Geoscience*, *9*(1), 46–50. https://doi.org/10.1038/ngeo2603

Tierney, J. E., & Tingley, M. P. (2018). BAYSPLINE: A new calibration for the alkenone paleothermometer. *Paleoceanography and Paleoclimatology*, *33*, 281–301. https://doi.org/10.1002/2017PA003201

Volkman, J. K., Eglinton, G., Corner, E. D. S., & Sargent, J. R. (1980). Novel unsaturated straight-chain C_{37}–C_{39} methyl and ethyl ketones in marine sediments and a coccolithophore *Emiliania huxleyi*. *Physics and Chemistry of the Earth*, *12*, 219–227. https://doi.org/10.1016/0079-1946(79)90106-X

Waelbroeck, C., Labeyrie, L., Michel, E., Duplessy, J. C., McManus, J. F., Lambeck, K., et al. (2002). Sea-level and deep water temperature changes derived from benthic foraminifera isotopic records. *Quaternary Science Reviews*, *21*(1-3), 295–305. https://doi.org/10.1016/S0277-3791(01)00101-9

Wang, L., Sarnthein, M., Erlenkeuser, H., Grimalt, J., Grootes, P., Heilig, S., et al. (1999). East Asian monsoon climate during the Late Pleistocene: High-resolution sediment records from the South China Sea. *Marine Geology*, *156*(1-4), 245–284. https://doi.org/10.1016/S0025-3227(98)00182-0

Wang, Y., Cheng, H., Edwards, R. L., He, Y., Kong, X., An, Z., et al. (2005). The Holocene Asian Monsoon: Links to solar changes and North Atlantic climate. *Science*, *308*(5723), 854–857. https://doi.org/10.1126/science.1106296

Wang, Y. J., Cheng, H., Edwards, R. L., An, Z. S., Wu, J. Y., Shen, C. C., & Dorale, J. A. (2001). A high-resolution absolute-dated Late Pleistocene monsoon record from Hulu Cave, China. *Science*, *294*, 2345–2348. https://doi.org/10.1126/science.1064618

Wang, Y. V., Leduc, G., Regenberg, M., Andersen, N., Larsen, T., Blanz, T., & Schneider, R. R. (2013). Northern and southern hemisphere controls on seasonal sea surface temperatures in the Indian Ocean during the last deglaciation. *Paleoceanography*, *28*, 619–632. https://doi.org/10.1002/palo.20053

Weber, M. E., Wiedicke-Hombach, M., Kudrass, H. R., & Erlenkeuser, H. (2003). Bengal Fan sediment transport activity and response to climate forcing inferred from sediment physical properties. *Sedimentary Geology*, *155*, 361–381. https://doi.org/10.1016/S0037-0738(02)00187-2

Yancheva, G., Nowaczyk, N. R., Mingram, J., Dulski, P., Schettler, G., Negendank, J. F. W., et al. (2007). Influence of the Intertropical Convergence Zone on the East Asian monsoon. *Nature*, *445*(7123), 74–77. https://doi.org/10.1038/nature05431

Yu, Z., Colin, C., Ma, R., Meynadier, L., Wan, S., Wu, Q., et al. (2018). Antarctic Intermediate Water penetration into the Northern Indian Ocean during the last deglaciation. *Earth and Planetary Science Letters*, *500*, 67–75. https://doi.org/10.1016/j.epsl.2018.08.006